GEOMETRIC PROCESSING OF VOLUMETRIC OBJECTS

Romildo Silva[1]

Jonas Gomes[2]

Cicero Mota[3]

[1]Departamento de Matemática – Universidade Federal do Ceará, 60455-760, Brazil
[2]VISGRAF Laboratory – Instituto de Matemática Pura e Aplicada, 22460-320, Brazil
[3]Instituto de Ciências Exatas – Universidade do Amazonas, 69077-000, Brazil.
{rjs, jonas, mota}@impa.br

ABSTRACT

This paper introduces techniques of Riemannian geometry for processing and visualising volumetric graphical objects. A family of non-linear high-pass filters, based on the curvature tensor, is introduced and used to study the local redundancy on objects. It is shown how to reconstruct an object from geometric non-redundant regions and applications are presented and discussed.

Keywords: Volumetric objects, processing, coding

1 INTRODUCTION

The output data for a great number of processes are volumetric. Computer tomography, magnetic resonance, seismic data and movies are important examples of this class of data. Nevertheless, most techniques from computer graphics are related to two-dimensional objects. This is in part, due to limitations imposed by the hardware. Today, technical advances in memory and processing capabilities of computers are favouring the appearance of new methods of visualisation and processing of volumetric objects.

In this work we introduce techniques from Riemannian geometry in the analysis of volumetric objects. This technique allows one to construct a family of nonlinear filters which are scale invariant and allow for reconstruction. Although some of the results in this paper could be obtained by linear filtering, the use of geometry is motivated by recent advances in human vision, [Koend87, Barth98]. The physical properties of our environment are related to strong geometric restrictions in volumetric objects. Motion, e.g., is related to zero Gaussian curvature. Differential geometry can be regarded as a strong tool for analysis of redundancy in such objects.

2 VOLUMETRIC OBJECTS

A *volumetric graphical object* is a pair (U, f), where U is a tridimensional subset of $\mathbb{R}^3$ called the *geometrical support* for the object and $f : U \to \mathbb{R}^n$ is an *attribute function*. The set U encloses the shape of the object, that is, its topology and geometry, while the attribute function deals with the other properties as, for example, colours, density, temperature etc. The volumetric graphical object is *scalar* if its attribute function takes values in $\mathbb{R}$.

2.1 Differential geometry and volumetric objects

From a geometrical viewpoint, we can describe a volumetric object as Monge surface:

$$\mathcal{S} = \{(x, y, z, f(x, y, z)) \mid (x, y, z) \in U\}. \qquad (1)$$

When f is a differentiable function, the Monge patch will be a differentiable surface whose parametrisation $F : U \to \mathcal{S}$ is given by

$$F(x, y, z) = (x, y, z, f(x, y, z)). \qquad (2)$$

We will use this parametrisation to calculate curvatures and other geometrical attributes, but

these attributes do not depend on a particular parametrisation.

The attribute function f can be interpreted as a singular immersion of $\mathcal{S}$ in $\mathbb{R}^n$. This provides an alternative way to study the volumetric graphical object by using differential geometry, not further pursued here.

In the following we present some elements necessary for the analysis and coding of a volumetric object by using differential geometry. The classical notation will also be introduced. From hereafter, we denote the partial derivatives of f by f_x, f_y, f_z, f_{xy}, etc.

2.2 The Gauss Map

The vectors F_x, F_y and F_z, given below, form a basis for the tangent plane of $\mathcal{S}$:

$$F_x = (1, 0, 0, f_x), \cdots, F_z = (0, 0, 1, f_z). \quad (3)$$

An unit vector field N, normal to $\mathcal{S}$, that defines an application from $\mathcal{S}$ to the unit sphere S^3 is called *Gauss map*.

A straightforward computation shows that, under the canonical parametrisation, the Gauss map is given by

$$N(p) = (-f_x, -f_y, -f_z, 1)/\sqrt{1 + \|\nabla f\|^2}\,. \quad (4)$$

Equation (4) shows that the Gauss map is differentiable. As usual, we indicate this derivative by N'_p. Since the tangent spaces $T_p\mathcal{S}$ and $T_{N(p)}S^3$ are coincident, N'_p is a linear operator from $T_p\mathcal{S}$.

It is a well known and fundamental fact that the differential N'_p of the Gauss map is selfadjoint. Therefore, one can compute an orthonormal basis with eigenvectors $\{e_1, e_2, e_3\}$ and eigenvalues $\lambda_1, \lambda_2, \lambda_3$ such that $N'_p(e_i) = \lambda_i e_i$ for $i = 1, 2, 3$.

The eigenvectors e_i are called *main directions* and the eigenvalues λ_i are the *main curvatures*. The symmetric functions of $\lambda_1, \lambda_2, \lambda_3$ have also special names: $K = \lambda_1\lambda_2\lambda_3$ is the *Gauss-Kronecker curvature*; $H = \lambda_1 + \lambda_2 + \lambda_3$ is the *mean curvature*; and $S = \lambda_1\lambda_2 + \lambda_1\lambda_3 + \lambda_2\lambda_3$ is called *scalar curvature*.

Of course, the matrix of N'_p with respect to the basis $\{e_1, e_2, e_3\}$ is given by $D = \mathrm{diag}(\lambda_1, \lambda_2, \lambda_3)$.

Let $A = (a_{ij})$ be a matrix for N'_p with respect to a given basis in $T_p\mathcal{S}$. It is a fact from linear algebra that the polynomial $P(x) = \mathrm{Det}(A - xI)$, (where I is the identity matrix) does not depend on a particular matrix representation of N'_p. Therefore, after computing and comparing this polynomial for both matrix A and D, we have:

$$\begin{aligned} K &= |A| \\ S &= \begin{vmatrix} a_{11} & a_{12} \\ a_{21} & a_{22} \end{vmatrix} + \begin{vmatrix} a_{11} & a_{13} \\ a_{31} & a_{33} \end{vmatrix} + \begin{vmatrix} a_{22} & a_{23} \\ a_{32} & a_{33} \end{vmatrix} \\ H &= a_{11} + a_{22} + a_{33} \end{aligned} \quad (5)$$

where $|\ .\ |$ denotes the determinant.

The above formulas enables one to compute the curvatures K, S and H from any matrix representation of N'_p and will be used for the applications presented in this work.

2.3 The Gauss Map and the Hessian

The differential of the Gauss map plays a fundamental role in the calculus of redundant regions of a volumetric graphical object. In this work, we use the rank of the Gauss map differential to classify the points of a volumetric object. This classification enables one to distinguish different kinds of redundancy.

Now, we show how to compute the matrix $A = (a_{ij})$ of the Gauss map's differential with respect to the basis given in (3). For this particular basis we can write:

$$\begin{aligned} N_x &= a_{11}F_x + a_{12}F_y + a_{13}F_z \\ N_y &= a_{21}F_x + a_{22}F_y + a_{23}F_z \\ N_z &= a_{31}F_x + a_{32}F_y + a_{33}F_z \end{aligned} \quad (6)$$

where, e.g., $N_x = N'_p(F_x), \ldots$

The derivative of $\langle N, F_x\rangle = 0$ with respect to x, gives us $\langle N_x, F_x\rangle + \langle N, F_{xx}\rangle = 0$. Proceeding the same way for y and z, we have:

$$\begin{aligned} \langle N_x, F_x\rangle &= -\langle N, F_{xx}\rangle \\ \langle N_x, F_y\rangle &= -\langle N, F_{yx}\rangle \\ \langle N_z, F_z\rangle &= -\langle N, F_{zz}\rangle \end{aligned} \quad (7)$$

From the above equalities and the expressions of F_x, F_y, F_z and N, we can write once more equation (6):

$$\mathrm{Hess}(f) = AM \quad (8)$$

where $M = \sqrt{1 + \|\nabla f\|^2}(I + \nabla f^T \nabla f)$ and $\mathrm{Hess}(f) = (f_{xx}, \ldots; \ldots; \ldots, f_{zz})$ is the symmetric matrix associated to the second derivative f'' with respect to the canonical basis of $\mathbb{R}^3$.

In this way, we have a relationship between the differential of the Gauss map and the second derivative of f. Since M is invertible because $\mathrm{Det}(M) = (1 + \|\nabla f\|^2)^{5/2} \neq 0$, we can compute the matrix for the Gauss map differential. In particular, this matrix and the Hessian have the same rank, and consequently the same number of nonzero eigenvalues.

3 NON-LINEAR FILTERS

In this section, we present some non-linear geometric filters. These filters are derived from the classification of the points of a volumetric object given by the rank of the Gauss map differential.

3.1 Geometric classification

Given a scalar volumetric object (U, f), we classify the points in the geometric support U between four possible kinds accordingly to the rank of N'.

Definition 1. *We say that p is of type gnD if $rank(N'_p) = n$.*

We call the above classification of *geometric classification*. Accordingly to the classic notation of differential geometry, the points of kind *g0D* are also called *planar points*. The concept of planar point is related to the concept of flat point in mathematical morphology [Serra93]. This classification has been use by Barth, Caelli & Zetzsche for perceptual studies [Barth93], see also [Mota99].

There is one more important thing to salient concerning the rank of the Gauss map differential. To compute it, we do not have to explicitly show the eigenvalues for N'_p. The knowledge of the curvatures K, S and H together gives the geometrical classification for the points of a volumetric object. That is what the following proposition states.

Proposition 1. *For any hypersurface $\mathcal{S}$ in $\mathbb{R}^4$, we have:*

1. *N'_p has rank 0 $\iff$ $H = K = S = 0$;*
2. *N'_p has rank 1 $\iff$ $K = S = 0$ e $H \neq 0$;*
3. *N'_p has rank 2 $\iff$ $K = 0$ e $S \neq 0$;*
4. *N'_p has rank 3 $\iff$ $K \neq 0$.*

The demonstration follows immediately from the definition of the curvatures H, K, S and from the fact that the rank of a diagonalisable matrix is equal to its number of non-zero eigenvalues.

Regarding implementation, we shall remark:

- The equalities in (5) give formulas to calculate the curvatures K, S and H from the matrix of N'_p in any basis of $T_p\mathcal{S}$. By proposition 1, one can compute the rank of the Gauss map differential from these curvatures.
- Equation (8) shows that the Gauss map's differential and the Hessian have the same rank, and therefore the same number of non zero eigenvalues. It follows that the geometric classification can be done in function of the Hessian instead of the Gauss map differential.

Although both the Gauss map differential and Hessian should give the same result, for a matrix representation of a volumetric graphical object, the Hessian appears to produce a more stable geometric classification.

3.2 Filtering

For a scalar volumetric graphical object (U, f) with Monge surface $\mathcal{S}$, the variation of the Gauss map along $\mathcal{S}$ is related to the variation of the attribute function f.

Let p be a point in $\mathcal{S}$, λ an eigenvalue for N'_p and v an eigenvector in $T_p\mathcal{S}$ associated to λ. If $\lambda \neq 0$, then $N'_p(v) = \lambda v \neq 0$, that is, the Gauss map varies along the direction of v and, therefore, the attribute function has a non-linear variation along the direction $u = \pi(v)$. Here, $\pi : \mathbb{R}^4 \longrightarrow \mathbb{R}^3$ is the canonical projection given by $\pi(x_1, x_2, x_3, x_4) = (x_1, x_2, x_3)$.

Let v_1 and v_2 be two orthonormal eigenvectors for N'_p associated to the non zero eigenvalues λ_1 and λ_2. Then, the Gauss map varies along all directions in the plan determined by p and by the vectors v_1, v_2. In fact, given a non-zero vector $v = \mu v_1 + \nu v_2$ in $T_p\mathcal{S}$, we have

$$N'_p(v) = N'_p(\mu v_1 + \nu v_2) = \mu\lambda_1 v_1 + \nu\lambda_2 v_2 \neq 0.$$

Consequently, the attribute function f has a non-linear variation along the direction $\pi(v) = \mu\pi(v_1) + \nu\pi(v_2)$. We can continue in this way and conclude that if all eigenvalues of N'_p are non

zero then f has variation along all directions passing through $\pi(p)$. Therefore, the regions *g0D* is an union of patches where the Gauss map is constant. It means that the attribute function has linear variation in these regions. The components *g1D*, *g2D* e *g3D* are regions where the volumetric object has non-linear variation.

The number of directions where the object varies increases with the index of the regions. Strong variations in the Gauss map are related to strong variations in the volumetric graphic object. Therefore, the geometric classification introduced in section 3.1 enables one to construct non-linear filters for detection of high frequency regions in a volumetric graphical object. Now, we define the filters to be used in the processing of volumetric objects in this work.

We denote by $\mathcal{F}_0$ the filter that makes correspond to every object (U, f) the object $(U, \mathcal{F}_0 f)$ given by

$$\mathcal{F}_0 f(p) = \begin{cases} f(p), & \text{if } p \text{ is of kind } g0D; \\ \text{med}(f), & \text{otherwise} \end{cases} \quad (9)$$

where $\text{med}(f)$ is the mean of the attribute function along U.

The filter $\mathcal{F}_0$ preserves the values of the attribute function along planar regions. In a similar way, we can define filters $\mathcal{F}_1$, $\mathcal{F}_2$ and $\mathcal{F}_3$, which preserve the values of the attribute function along *g1D*, *g2D* and *g3D*, respectively.

It is possible to use combinations of the regions in the geometric classification to construct others filters. For example, $\mathcal{F}_{123}$ given by

$$\mathcal{F}_{123} f(p) = \begin{cases} \text{med}(f), & \text{if p is of type } g0D; \\ f(p), & \text{otherwise} \end{cases} \quad (10)$$

This filter will be used in section 4, where we deal with the coding and reconstruction problems. The filter $\mathcal{F}_{123}$ preserves values of the attribute function along the components *g1D*, *g2D* and *g3D*. Planar points are changed to the mean of the attribute function.

Consider now the filter $\mathcal{G}_{123}$ given by

$$\mathcal{G}_{123} f(p) = \begin{cases} 0, & \text{if } p \text{ is of type } g0D; \\ 1, & \text{otherwise} \end{cases} \quad (11)$$

The filter $\mathcal{G}_{123}$ is called *planar discrimination filter*. It discriminates between planar and non-planar regions of the volumetric graphical object.

The geometric classification introduced in section 3.1 do not depend on a particular system of coordinates. The same is true for the geometric filters presented. This guarantees that these are isotropic filters. They find high frequencies in any direction of the volumetric graphical object.

3.3 Examples

In the following we show two examples of geometric filtering. We will use the geometric filter $\mathcal{G}_{123}$ introduced in (11). In these examples the number 1 means black while the number 0 means white. By the definition of the planar discrimination filter $\mathcal{G}_{123}$, the white colour corresponds to planar regions and the black colour to non-planar regions.

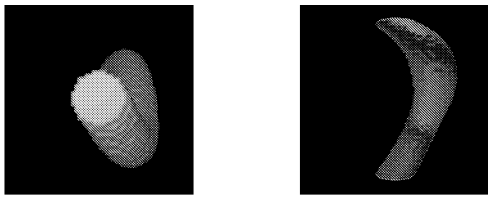

(a) view xy (b) view xz

Figure 1: A volumetric graphical object constructed moving a disc along a curve

Example 1. The body in figure 1 was constructed moving a disc along a curve which connects two points in opposite faces of a cube. Figure 2 shows eight consecutive transversal sections of the original object (first row). Down in the same figure, we can see the high frequencies regions detected by the filter $\mathcal{G}_{123}$ (second row).

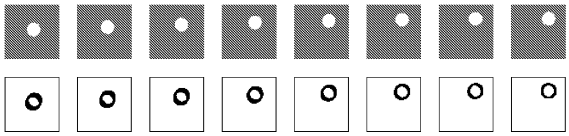

Figure 2: Transversal sections: the original object and its filtered version.

Example 2. A *video* is a one-parameter family of images $f_t : U \to \mathbb{R}^3$, where U is a two-dimensional subset of R^2 and the time variable t belongs to the unit interval. Therefore, video can be interpreted in the volumetric graphical object paradigm, the geometric techniques described provides a tool for video processing. In this way, the video is seen as whole body instead of simply as an image sequency. Figure 3.3 shows a video segment (first line) jointly with its filtered version (second line). Filtering was done with the

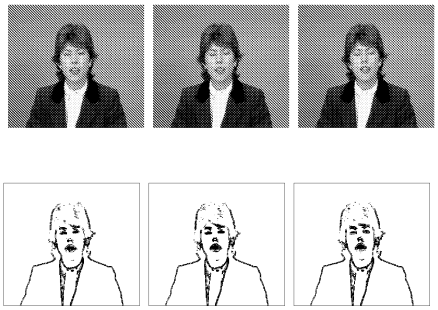

Figure 3: A video segment and its geometric filtered version.

geometric filter $\mathcal{G}_{123}$. We can see, in the filtered version, the high frequencies regions of the video segment. The geometric processing of videos has been used in [Silva99] to study the *video cut detection* problem. In that work, the authors show that the number of planar points for continuous segments of video is almost constant and changes subtly at edition points. The resulting algorithm was shown to be very robust and performs in real time.

3.4 Scale invariance

An important property for a decomposition of an object is *scale invariance*. In this section we show that the geometric classification has this property.

Given a volumetric graphical object (U, f) and $\Lambda = (\lambda, \mu, \nu)$ positive, let ψ_Λ be the transformation given by $\psi_\Lambda(x, y, z) = (\lambda x, \mu y, \nu z)$, $U_\Lambda = \psi_\Lambda^{-1}(U)$ and $\mathcal{P}_\Lambda$ the *scale operator*, that is,

$$\mathcal{P}_\Lambda f = f \circ \psi_\Lambda. \tag{12}$$

Proposition 2. *The scale operator preserves the geometric classification. That is, given a geometric graphical object (U, f) and its scaled version $(U_\Lambda, f \circ \psi_\Lambda)$, then p and $\psi_\Lambda(p)$ are of the same geometric type.*

Proof. Let $g = \mathcal{P}_\Lambda f$. By definition, for every point $p = (x, y, z)$ in U_Λ we have

$$g(x, y, z) = f \circ \psi_\Lambda(x, y, z) = f(\lambda x, \mu y, \nu z).$$

The above equality gives us

$$\text{rank}(\text{Hess}(g)(p)) = \text{rank} \begin{pmatrix} \lambda^2 f_{xx}(q) & \lambda\mu f_{xy}(q) & \lambda\nu f_{xz}(q) \\ \lambda\mu f_{yx}(q) & \mu^2 f_{yy}(q) & \mu\nu f_{yz}(q) \\ \lambda\nu f_{zx}(q) & \mu\nu f_{zy}(q) & \nu^2 f_{zz}(q) \end{pmatrix} =$$

$$\text{rank} \begin{pmatrix} \lambda f_{xx}(q) & \mu f_{xy}(q) & \nu f_{xz}(q) \\ \lambda f_{yx}(q) & \mu f_{yy}(q) & \nu f_{yz}(q) \\ \lambda f_{zx}(q) & \mu f_{zy}(q) & \nu f_{zz}(q) \end{pmatrix} =$$

$$\text{rank}(\text{Hess}(f)(q)).$$

By definition, the geometric classification of a point in an object is given by the rank of the Gauss map differential at this point. We have seen in section 3.1 that the Hessian of the attribute function of an object and the Gauss map's differential of its associate Monge surface have the same rank. Since the matrix $\text{Hess}(g)(p)$ and $\text{Hess}(f)(\psi_\Lambda(p))$ have the same rank, it follows that p and $\psi_\Lambda(p)$ have the same geometric classification. But p can be any point in U_Λ, which shows that the scale operator $\mathcal{P}_\Lambda$ preserves the geometrical classification. □

The above result can be used to show that the percentage of planar points in a photogram does not depend on a particular resolution of a video, see [Silva99].

4 EXACT RECONSTRUCTION

In this section, we deal with the issue of coding and reconstruction of a volumetric graphical object using differential geometry techniques. We show how to reconstruct an object from its $\mathcal{F}_{123}$ filtered version.

A proof of the redundancy of points of kind $g0D$ and $g1D$ as well as an algorithm for reconstructing from the remaining $g2D$ points has been presented in [Mota00]. Since the math used in that proof is too technical, we present here a simplified proof that applies only to the redundancy of points of kind $g0D$.

Theorem 1. *A hypersurface in $\mathbb{R}^4$ is completely determined by its set of non-planar points.*

Proof. The set of non-planar points is a collection of connected plan patches. If $\mathcal{S}' = \{p \in \mathcal{S} \mid N'_p \neq 0\}$ and $p \in \partial\mathcal{S}'$, the plan patch π_p that has a common border with $\mathcal{S}'$ at p has $N(p)$ as normal vector. But π_p is completely determined by p and $N(p)$, follows that $\mathcal{S}$ is determined by $\mathcal{S}'$. □

4.1 A reconstruction algorithm

The difficulty in reconstructing a volumetric object from its filtered version comes from the non-linearity of geometric filters. This problem for linear filters is more easy since one only has to solve

a system of linear equations. To reconstruct a volumetric object from its filtered version $(U, \mathcal{F}_{123}f)$ we have to reconstruct the planar regions. In principle, one can think of a simple scan line algorithm to reconstruct the object. But, this is not exactly the case because in the classification process we have to use some threshold and not exactly planar regions may be classified as planar ones. This with the natural noisy present in objects prevents a pure scan line algorithm from correctly reconstruct the surface. The key to a better reconstruction algorithm resides in seeing planar patches as harmonic functions. We describe now an algorithm for reconstruction.

Let $[f_{ijk}]$ be a matrix representation of the object. If a voxel (i, j, k) belongs to the planar regions of the object, the attribute function must satisfy the equation

$$\begin{aligned} f_{ijk} =& \frac{1}{6}\{f_{i-1jk} + f_{i+1jk} + f_{ij+1k} \\ &+ f_{ij-1k} + f_{ijk+1} + f_{ijk-1}\}. \end{aligned} \tag{13}$$

The above equality is the main motivation for the reconstructing algorithm we present below.

Let $g = \mathcal{F}_{123}f$ be the filtered version of f. Using the geometric classification of the points in the support of (U, f), the following operation is done for each voxel in the matrix representation of g:

1. Proceed with a scan line reconstruction to obtain a first version of g.
2. If the voxel (i, j, k) is planar, then change g_{ijk} according to equation 13.
3. If the voxel (i, j, k) is not planar, keep the value for g_{ijk}.
4. Go to step 2.

This algorithm reconstructs the attribute function of a geometric graphical object along planar regions. For each iteration, the algorithm reconstructs the object from the border to the inner of missing regions. It is a interpolation process that makes reconstructed regions with variation close to linear along regions classified as planar.

4.2 Convergence of the algorithm

Now, we will show that the previous algorithm is convergent and consequently it reconstructs the volumetric graphical object.

We justify the algorithm's convergence by the analysis of the unidimensional case. In this case, the problem consist in reconstructing a linear function $L : [0, n] \to \mathbb{R}$ at nodes $1, \ldots, n-1$, from $g : [0, n] \longrightarrow \mathbb{R}$ with values $g(0) = L(0) = a$, $g(1) = \cdots = g(n-1) = c$ e $g(n) = L(n) = b$, using the pseudo-code below, see figure 4.

```
while( Number_of_Iteration-- )
{
   for(i=1; i<n; ++i)
      g[i] = ( g[i-1] + g[i+1] )/2;
}
```

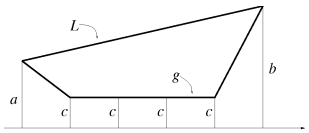

Figure 4: The graphic for L and g.

Given the finite sequence $y^0 = (a, c, \ldots, c, b)$, let for every $k \geq 1$ the finite sequence y^k be given by

$$\begin{aligned} y_0^k &= a \\ y_i^k &= \frac{y_{i-1}^k + y_{i+1}^{k-1}}{2} \quad i = 1, \ldots, n-1 \\ y_n^k &= b \end{aligned} \tag{14}$$

Figure 5 shows how these sequences are built for $c = 0$ and $n = 5$. To proof that the algorithm converges, we have to show that, for every i, the infinite sequence y_i^k converges to $L(i)$, when k goes to infinity. Let $g^k : [0, n] \longrightarrow \mathbb{R}$ be the function given by linear interpolation of $(0, y_0^k), \ldots, (n, y_n^k)$.

One can easily proof that y_i^k converges to $L(i)$, for all i, if and only if the sequence of functions g^k converges to the linear function L on the interval $[0, n]$.

Proposition 3. *The sequence of functions $g^k : [0, n] \longrightarrow \mathbb{R}$ converges to the linear function $L : [0, n] \longrightarrow \mathbb{R}$.*

Proof. We can suppose without loss of generality that $c = 0$. We first show that, for every i, the sequence y_i^k defined in (14) converges, that is, there

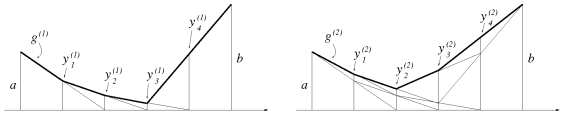

Figure 5: Building of g^1, g^2, ...

exist y_i such that $y_i^k \longrightarrow y_i$ when $k \longrightarrow \infty$. To accomplish this, it is sufficient to proof the convergence for the cases $a = 0$ or $b = 0$. In fact, Let u^k and v^k be the sequences, as in (14) with $a = 0$ and $b = 0$, respectively.

Figure 6 shows the construction for sequences u^k when $n = 5$. It is not hard to see that, for every i,

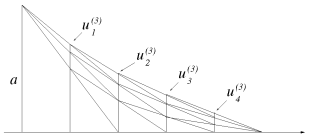

Figure 6: Sequences u_i^k.

u_i^k e v_i^k are bounded monotone sequences. Therefore, they are convergent. Let $u_i = \lim_{k\to\infty} u_i^k$ and $v_i = \lim_{k\to\infty} v_i^k$.

From the definition of u_i^k, v_i^k and y_i^k, we have

$$y_i^k = u_i^k + v_i^k.$$

Thus, for every i, the sequence y_i^k is the sum of two convergent sequences and consequently is itself a convergent sequence. Let be $y_i = \lim_{k\to\infty} y_i^k$, to complete the proof, we need only to show that $y_i = L(i)$.

For every $k \geq 1$ and $i = 1, \ldots, n-1$, we have by definition

$$y_i^k = \frac{y_{i-1}^k + y_{i+1}^{k-1}}{2}.$$

Going to the limits in the above equality results in

$$y_i = \frac{y_{i-1} + y_{i+1}}{2},$$

for every $i = 1, \ldots, n-1$. Therefore, we have

$$a - y_1 = y_2 - y_1 = \cdots = y_{n-1} - y_{n-2} = b - y_1,$$

from where one concludes that the points $(0, y_0), \ldots, (n, y_n)$ belong to the same straight line. Consequently,

$$y_i = L(i) \quad \text{for } i = 1, \ldots, n-1$$

and this concludes the proof. □

One can easily derive, from the above proposition, the convergence of the reconstruction algorithm for the three dimensional case.

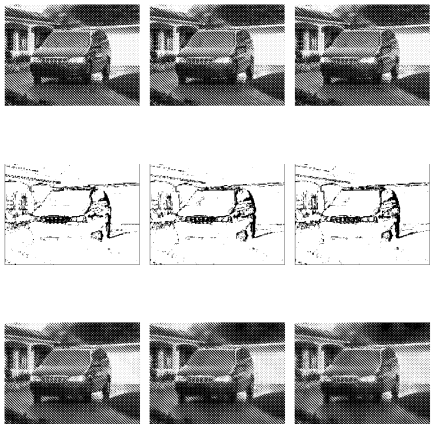

Figure 7: Reconstruction (40 iterations).

4.3 Examples

In this section we present some example of filtering and reconstruction of volumetric graphical objects from their non-planar regions. The algorithm described in the previous section was used for reconstructing the objects. For illustrating purposes, we have used the discriminating planar filter $\mathcal{G}_{123}$ in figures 7 and 8, that is, 0 (white) for planar points and 1 (black) for non-planar ones. The reconstruction was done with the geometric filter $\mathcal{F}_{123}$. This filter preserves the attribute function along non-planar regions.

4.3.1 Video

Consider the image sequence shown in figure 7. Second row shows the filtered sequence computed using the discriminating planar filter $\mathcal{G}_{123}$. The derivatives were estimated with quadratic reconstruction and points were classified using the Hessian instead of the Gauss map differential. Third row shows the reconstructed object after 40 iterations.

4.3.2 Medical data

The first row of figure 8 presents consecutive transversal sections of a volumetric object originated from computer tomography [Avila96]. The attribute functions for this kind of object is highly non-homogeneous. Second row shows the $\mathcal{G}_{123}$ filtered version of the object. Note the presence of planar regions (white). The reconstruction is presented in third row.

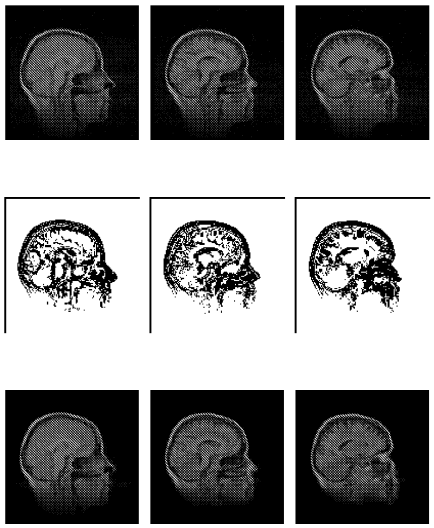

Figure 8: Reconstruction (40 iterations).

5 FUTURE WORK

In this section we will discuss some possible extensions of the work presented in this paper and some interesting potential applications of the geometric filters introduced here.

5.1 Multi-scale reconstruction

Since geometric filters are invariant by scale change, we have the possibility to explore a multi-scale reconstruction algorithm. Thus, with a given representation using the geometric filter, we can reconstruct the original volumetric object in different scales. Besides the possibility of obtaining a more efficient reconstruction algorithm, the multi-scale reconstruction can be useful for applications where decisions could be made based on coarse scaled copies of the object.

5.2 Mesh refinement and simplifications

We can use the geometric filters introduced in this work to make the simplification and refinement of surface triangulation and, as a extension, the construction and simplification of volumetric object triangulation.

ACKNOWLEDGEMENTS

We thank E. Barth for comments on the the manuscript. R. S. thanks the Brazilian Research Agency CAPES for partial support. C. M. thanks the Institute for Signal Processing, Medical University of Luebeck where this work has been finished.

REFERENCES

[Avila96] Avila, R., He, T., Hong, L., Kaufman, A., Pfister, H., Silva, C., Sobierajskiand, L., Wang, S.: *VolVis: A Diversified Volume Visualisation System*, State University of New York at Stony Brook, 1996.

[Barth93] Barth, E., Caelli, T., Zetzsche, C.: *Image Encoding, Labelling, and Reconstruction from Differential Geometry, CVGIP: Graphical Models and Image Processing*, Vol. 55, pp. 428–446, 1993.

[Barth98] Barth, E., Zetzsche, C., Krieger, G.: *Curvature Measures in Visual Information, Open Sys. & Information Dyn.*, Vol. 5, pp. 25–39, 1998.

[doCar88] do Carmo, M. P.: *Geometria Riemanniana*, Projeto Euclides, Instituto de Matemática Pura e Aplicada (IMPA), 1988.

[Koend87] Koenderink, J. J., van Doorn, A. J.:*Representation of local geometry in the visual system, Biol. Cybern.*, Vol. 55, pp. 367–375, 1987.

[Mota99] Mota, C.: *Geometric Image Processing*, Phd thesis, Instituto de Matemática Pura e Aplicada (IMPA), In Portuguese, 1999.

[Mota99b] Mota, C., Gomes, J. *Curvature Operators in Geometric Image Processing, Proceedings of XII Brazilian Symposium on Computer Graphics and Image Processing*, IEEE Computer Society Press, 1999.

[Mota00] Mota, C., Barth, E.: *On the Uniqueness of Curvature Features, Proceedings in Artificial Intelligence (Dynamische Perzeption)*, Vol. 9, pp. 175–178, Infix Verlag, 2000.

[Serra93] Serra, J., Salembier, P.: *Connected Operators and Pyramids, Proceedings of SPIE*, Vol. 2030, pp. 65–76, 1993.

[Silva99] Silva, R. J., Gomes, J., Velho, L.: *Video Cut Detection Using Volumetric Image Sequence Processing, Proceedings of EUROGRAPHICS*, 1999.